Journal of Power Sources 249 (2014) 306–310

Contents lists available at ScienceDirect

Journal of Power Sources

journal homepage: www.elsevier.com/locate/jpowsour

Short communication

High capacity and cyclic performance in a three-dimensional composite electrode filled with inorganic solid electrolyte

Kai Chen, Yang Shen*, Yibo Zhang, Yuanhua Lin, Ce-Wen Nan*

State Key Laboratory of New Ceramics and Fine Processing, School of Materials Science and Engineering, Tsinghua University, Beijing 100084, PR China

HIGHLIGHTS

- Surface capacity of ~9 mAh cm^{-2} is obtained.
- Excellent cycling performance and good rate capability at various discharge rates.
- The novel composite cathodes are highly compact with a relative density of 92%.
- No electronic conductive additive or polymer binder is used.
- The one-step sintering approach may be readily applied to other cathode systems.

ARTICLE INFO

Article history:
Received 16 August 2013
Received in revised form
18 October 2013
Accepted 24 October 2013
Available online 5 November 2013

Keywords:
Three-dimensional composite electrode
Lithium ion battery
Specific capacity
Solid state electrolyte
All solid state battery

ABSTRACT

Three-dimensional (3-D) composite electrodes are prepared by one-step sintering of the laminated $LiCoO_2$ and 0.44LiBO2·0.56LiF pellets, in which the amorphous 0.44$LiBO_2$·0.56LiF solid electrolyte melts during the sintering process and fills the interspaces in the underlying highly conductive 3-D frame formed by $LiCoO_2$. The one-step sintering process yields a compact electrode structure of ~92% in relative density, which contains no electronic conductive additives or polymer binder. For better characterization of the composite electrode, liquid electrolyte is used in the battery test, but the vast majority of the active material is in the all-solid-state environment. The specific capacity of the 3-D composite electrode is dependent on the thickness of the composite electrodes. The 100-μm-thick 3-D composite electrode possesses high specific discharge capacity of 131 mAh g^{-1} at C/20 rate (96% utilization of the active material), excellent cycling performance for the measured 20 cycles and good rate capability at various discharge rates. The 200-μm-thick 3-D composite electrode delivers 88% of the theoretical capacity, i.e., 120 mAh g^{-1}, and a significantly enhanced surface capacity of ~9 mAh cm^{-2}, which is much higher than that of the electrode used in the conventional all-solid-state lithium battery.

1. Introduction

Safety issues and substantial demand for higher energy density are two major challenges for the lithium ion batteries [1,2], which slow down their applications in electric vehicles and energy storage for power stations. All-solid-state lithium ion batteries, with solid state electrolytes and new battery structure designs, are the ultimate solution for the safety issues and have attracted ever-increasing attentions for the past few years. The thin film type all-solid-state batteries prepared by film deposition techniques have been thoroughly investigated [3–8]. Limited by the very thin cathodes employed, the surface capacities of these thin film type batteries are only 9.9–250 μAh cm^{-2}, though they could deliver excellent capacity retention over thousands of cycles [9]. Bulk-type all-solid-state batteries are thus considered more promising to be used in the scenarios where high capacity is crucial. In principle, the capacity and cycle lifetime of all-solid-state batteries are determined by the microstructure of the cathode especially the interfaces between the active cathode materials and the solid electrolytes. Recently, a number of efforts have been made in constructing porous cathodes with pores of three-dimensional (3-D) connectivity inside [10,11]. With the ionic electrolyte filled in the pores, these 3-D composite cathodes are capable of providing higher capacity due to their significantly larger specific areas and much shorter diffusion path for the lithium ions during the charging/discharging process. For instance, Lai et al. reported that porous 3-D $LiCoO_2$ electrode with liquid electrolyte filled-in

* Corresponding authors. Tel.: +86 10 62773587; fax: +86 10 62772507.
E-mail addresses: shyang_mse@tsinghua.edu.cn (Y. Shen), cwnan@tsinghua.edu.cn, cwnan@mail.tsinghua.edu.cn (C.-W. Nan).

0378-7753/$ – see front matter © 2013 Elsevier B.V. All rights reserved.
http://dx.doi.org/10.1016/j.jpowsour.2013.10.113

exhibited ultrahigh energy density and good cycling performance [12]. Thick film cathodes filled with solid oxide electrolyte have also been reported [13]. However, a composite of thick oxide electrolyte pellets of about 0.5–1 mm and thin cathode layer of only about 10 μm result in low capacity and energy density [13]. By increasing the thickness of the composite electrode to 400 μm, a higher surface capacity of 2.2 mAh cm^{-2} was achieved in a monolithic solid-state lithium battery with $Li_{1.5}Al_{0.5}Ge_{1.5}(PO_4)_3$ as solid electrolyte and $Li_3V_2(PO_4)_3$ as electrodes [14], which is much higher than that in the thin film type all-solid-state batteries. Another report on filling solid inorganic electrolyte into the open pores of the porous 3-D $LiCoO_2$ electrode was carried out by repeatedly infiltrating $Li_{0.35}La_{0.55}TiO_3$ sol into the pores of the pre-sintered $LiCoO_2$ substrate and the subsequent heat treatments. The 100-μm-thick electrode thus prepared could deliver a specific discharge capacity of only 115 mAh g^{-1}, and no cycling data was given [15]. Moreover, the infiltration and firing process needs to be repeated many cycles and is time-consuming and labor intense.

In this contribution, a high performance composite electrode is prepared via a simple one-step sintering process by using $LiCoO_2$ as active cathode material and $0.44LiBO_2 \cdot 0.56LiF$ as amorphous solid electrolyte. Instead of direct co-firing or infiltrating the porous cathode with precursor sol of solid electrolyte, laminated $LiCoO_2$ pellet and $0.44LiBO_2 \cdot 0.56LiF$ pellet was uni-axially pressed together, as shown in Fig. 1. With a melting temperature of <700 °C [16], $0.44LiBO_2 \cdot 0.56LiF$ solid electrolyte was melted during the sintering process at 950 °C and infiltrated the underlying $LiCoO_2$ frame. The one-step sintering process yielded a 3-D composite electrode of ~92% in relative density. Without any electronic conductive additive or polymer binder, the novel composite cathodes are highly compact as compared with their counterparts in the conventional liquid lithium battery. A rather high specific discharged capacity of 131 mAh g^{-1} (or a high surface capacity of 5 mAh cm^{-2}) was achieved in a 100-μm-thick composite electrode, which is up to 96% of the theoretical capacity of $LiCoO_2$ (137 mAh g^{-1}). Further increase in the thickness to 200 μm led to an even higher surface capacity of 9 mAh cm^{-2}. Given the low sintering temperature and the amorphous nature of $0.44LiBO_2 \cdot 0.56LiF$ solid electrolyte, this one-step sintering approach is promising to be extended to other cathode systems.

2. Experimental

Battery-grade $LiCoO_2$ powder was ball-milled for 12 h, and used as active material of the composite electrodes. $LiBO_2$ and LiF with a molar ratio of 0.44:0.56 were mixed using an agate mortar to act as solid ionic electrolyte. The active material and solid ionic electrolyte were pressed into pellets with a diameter of 12 mm, separately. Then the active material pellet and solid electrolyte pellet with a mass ratio of 2:1 were stacked as shown in Fig. 1a, and sintered at 950 °C for 90 min. During the sintering process, $LiCoO_2$ particles in the lower pellet connected together and formed a 3-D frame, while the upper pellet consisting of $LiBO_2$ and LiF melt and filled into interspaces of the $LiCoO_2$ frame (Fig. 1b), forming the 3-D composite electrode (Fig. 1c). For comparison, pure $LiCoO_2$ and $0.44LiBO_2 \cdot 0.56LiF$ pellets were also sintered under the same condition.

X-ray diffraction (XRD, Rigaku D/max-2500 diffraction meter with a Cu Kα radiation source) was used for the phase identification in the sintered composite electrode. The microstructure of the $LiCoO_2$ ceramics sintered with and without solid electrolyte was observed by scanning electron microscopy (SEM, JEOL JSM-7001F). The composition of the 3-D composite electrode was determined using inductively coupled plasma spectroscopy (ICP-AES, Varian Vista-MPX) and ion chromatography (IC, Metrohm 761 compact). Electrochemical impedance measurement was carried out with an impedance analyzer (ZAHNER-elektrik IM 6) in the frequency range from 100 kHz to10 mHz with an AC voltage amplitude of 5 mV.

As the first step towards the goal of all solid state battery, we focus on the preparation and evaluation of the composite electrode. In order to better test the performance of the composite electrodes, liquid electrolyte is used here, but the liquid electrolyte is only wetting the surface of the dense composite electrode and only some of $LiCoO_2$ particles on top surface could be contacting to the liquid electrolytes, and thus the vast majority of the active material inside the composite electrode is in the all-solid-state environment not contact with the liquid electrolyte (see Fig. 1c). In this scenario, Lithium ions as well as electrons are transported solely by the solid electrolyte and the $LiCoO_2$ inside the composite electrode. For battery measurement, the composite electrodes were polished to different thickness ranging from 100 μm to 500 μm. Au was sputtered onto one side of the composite electrode as the current collector. A piece of lithium foil was then pressed onto another collector, on top of which one layer of Celgard 2400 separator was placed. Then, the prepared composite electrode was centered over the separator. The whole laminated construction was sealed in a LIR 2032 cell with electrolyte solution of 1 M $LiPF_6$ dissolved in ethylene carbonate (EC) and diethyl carbonate (DEC) (1:1). The cells were galvanostatically cycled between 2.5 and 4.2 V vs. Li/Li^+ at C/20. For investigation of the rate capability of the 100-μm-thick 3-D composite electrode, CC charging was used, with constant current C/10 applied until cell voltage reached 4.2 V, after which cells were galvanostatically discharged at various rates to 2.5 V. Cyclic tests indicate that the $0.44LiBO_2 \cdot 0.56LiF$ solid electrolyte is stable against the liquid electrolyte solution (see Fig. S1 in the Supporting information).

3. Results and discussion

3.1. Structure and composition

Fig. 2 shows the XRD patterns of the fresh surface and interior of the sintered 3-D composite electrode. For the upper and lower fresh surfaces, diffraction peaks corresponding to $LiCoO_2$ (PDF 50-0653)

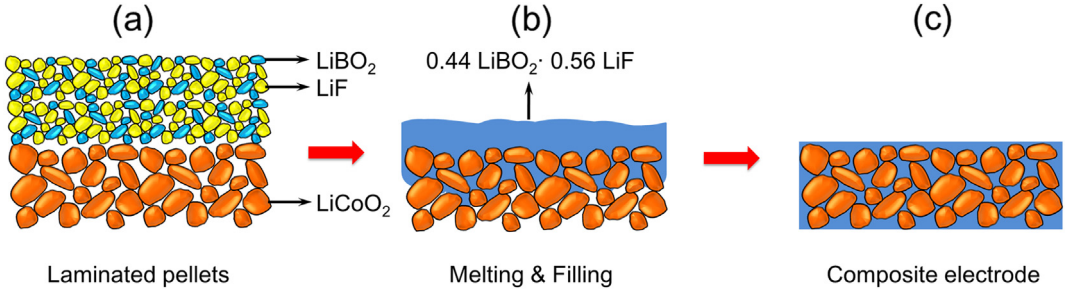

Fig. 1. A schematic illustration for the preparation process of the 3-D composite electrodes.

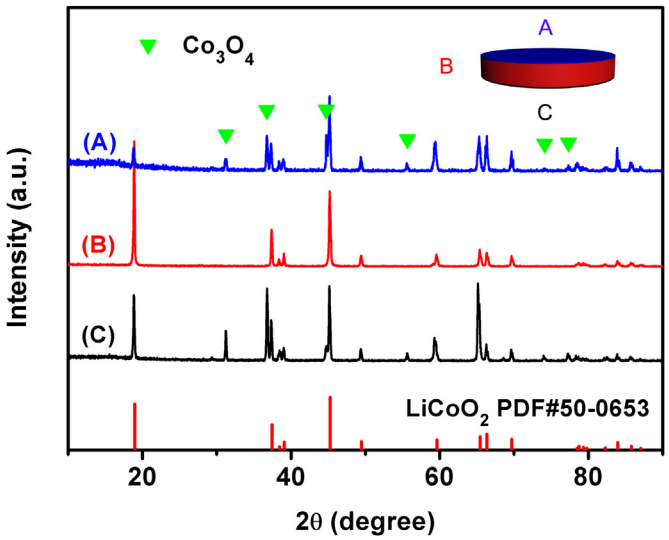

Fig. 2. XRD patterns for (A) upper fresh surface, (B) interior, and (C) lower fresh surface of the sintered 3-D composite electrodes.

and Co_3O_4 (PDF 42-1467) were observed. The appearance of Co_3O_4 phase at surfaces was due to the volatilization of Li during the sintering process. While for the interior, only pure $LiCoO_2$ diffraction peaks appeared. In the whole samples, no $LiBO_2$ or LiF diffraction peak could be observed in the XRD patterns of the fresh surfaces or interior of the composite electrode, which indicates that the solid ionic electrolyte was amorphous in the 3-D composite electrode.

As seen from the SEM micrographs of the pure $LiCoO_2$ pellet and the 3-D composite electrodes in Fig. 3, many pores existed in the interspaces of the connected $LiCoO_2$ particles in the pure $LiCoO_2$ pellet whose relative density was about 69% as determined by Archimedes method in ethanol, while no obvious pores can be observed in the 3-D composite electrodes with a relative density of 92%. The density increases notably in comparison with the pure $LiCoO_2$ pellet due to the introduction of the amorphous solid electrolyte. The comparison between their SEM micrographs in Fig. 3(a) and (b) also clearly illustrates that the amorphous solid electrolyte was infiltrated into the 3-D $LiCoO_2$ electrodes and the particles are mostly covered by the amorphous solid electrolyte. Fig. 3c also shows that the top surface of the composite electrode is covered by the amorphous solid electrolyte, as proposed in Fig. 1c. The mass fraction of $LiCoO_2$ in the composite electrode can be calculated as follows, i.e.,

$$\frac{m}{\rho_2} = \frac{m \times f}{\rho_1} + \frac{m \times (1-f)}{\rho_3} \quad (1)$$

$$f = \frac{\rho_1 \times (\rho_3 - \rho_2)}{\rho_2 \times (\rho_3 - \rho_1)} \quad (2)$$

where ρ_1, ρ_2, ρ_3 are the actual densities of $LiCoO_2$, composite electrode and solid electrolyte, respectively, as seen in Table 1; m and f are the mass of the composite electrode and the mass fraction of the $LiCoO_2$, respectively. Thus the calculated mass fraction of $LiCoO_2$ in the composite electrode is about 91.3%.

ICP and IC analysis were carried out to check the composition of the composite electrode and to verify the mass fraction of $LiCoO_2$ in the composite electrode. The molar ratio of elements in the composite electrode is about Li:Co:B:F = 5.76:4.87:0.437:0.563 measured by using ICP for Li, Co, and B, and using IC for F, which corresponds to 92.9 wt% $LiCoO_2$, 4.24 wt% $LiBO_2$ and 2.85 wt% LiF. This measured mass fraction of $LiCoO_2$ agrees well with that (91.3%) obtained from the density calculations above (inaccuracy < 2%). The molar ratio of $LiBO_2$ to LiF fits well with the composition in the raw materials. Lithium volatilization accounts for a bit loss of Li (<2%).

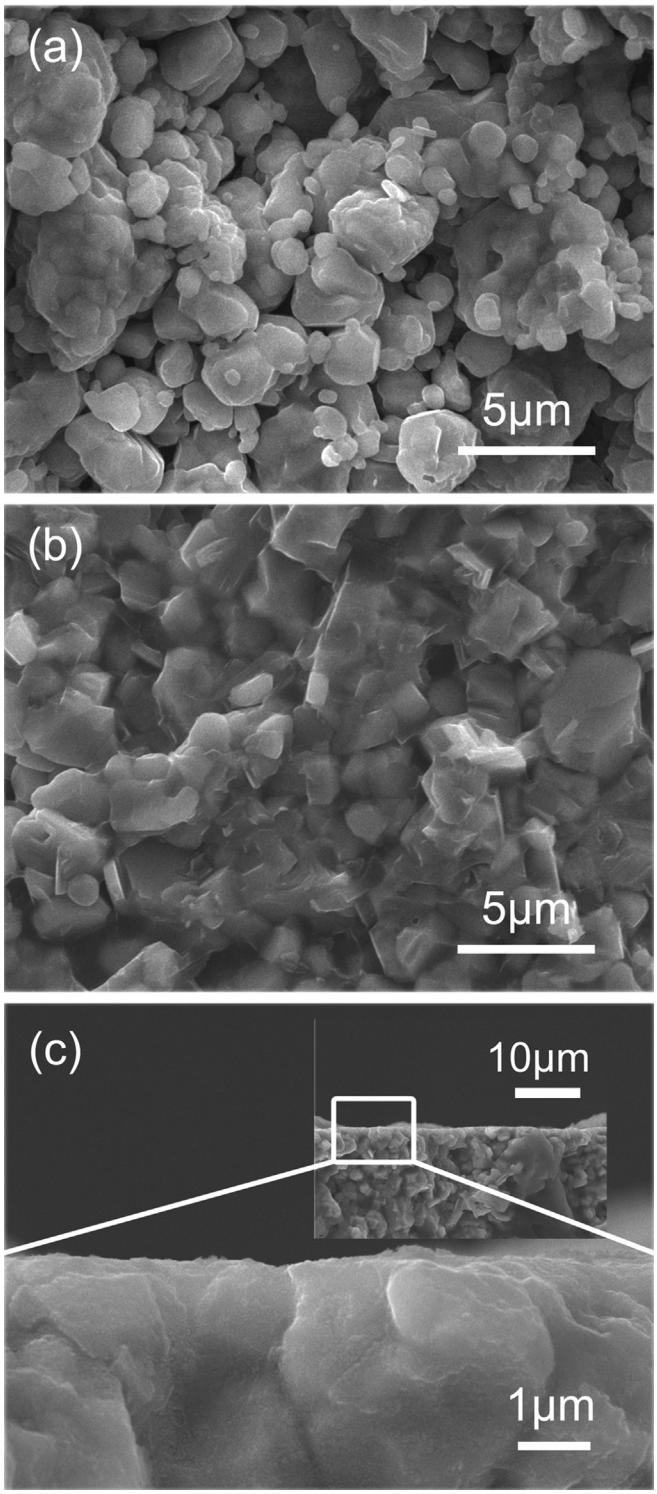

Fig. 3. SEM micrographs of the (a) fractured surface of pure $LiCoO_2$ pellet, (b) fractured surface of 3-D composite electrode; and (c) cross-sectional top surface of the 3-D composite electrode.

Table 1
The density of pure $LiCoO_2$ pellet, $0.44LiBO_2 \cdot 0.56LiF$ pellet and composite electrode pellet determined by Archimedes method in ethanol.

Sample	Apparent density g cm^{-3}	Relative density %	Actual density g cm^{-3}
Pure $LiCoO_2$ (ρ_1)	3.51	69	5.09
$0.44LiBO_2 \cdot 0.56LiF$ (ρ_3)	2.29	95	2.41
Composite electrode (ρ_2)	4.27	92	4.64

3.2. Electrochemical properties

Fig. 4a shows the first three charge/discharge cycles for a 100-μm-thick 3-D composite electrode. As can be seen, at C/20 rate, 96% utilization of the active material is obtained with a specific discharge capacity of 131 mAh g^{-1} (or a surface capacity of 5 mAh cm^{-2}). A small initial polarization spike was observed in the first charging process, which can be explained by partial delithiation of $Li_{1-x}CoO_2$. During the partial delithiation, $Li_{1-x}CoO_2$ undergoes a semiconductor–metal transition, with conductivity increasing dramatically [17]. And then the polarization phenomenon disappears in the following cycles.

The thickness of the composite electrodes plays a key role in determining the capacity and cycle lifetimes of the composite electrodes. As seen from Fig. 4b, the specific capacity and first cycle efficiency of the 3-D composite electrodes decrease with increasing the thickness of the composite electrode. This is especially so as the thickness is larger than 200 μm. Amorphous solid state electrolyte, i.e., $LiBO_2$ and LiF, acts as the ionic conductor between the $LiCoO_2$ frames in the 92% dense composite electrode, which guarantees high ionic conductivity of the composite electrolyte (as could be observed from the impedance spectra shown in Fig. S2 in the Supporting information). The ionic conductivity of 0.44 $LiBO_2 \cdot$ 0.56 LiF solid electrolyte is about 10^{-6} S cm^{-1} [16]. With no electronic conductive additives added in the composite electrode, the transport paths for electrons are only provided by the highly conductive $LiCoO_2$ frames and these paths are much longer than those in the conventional liquid lithium battery, considering the compact structure of the composite electrode. And with increasing thickness, the charging/discharging current density increases at the same cycling rate. Thus, the polarization of the composite electrode becomes more distinctive with increasing thickness of the electrode, resulting in decline of the specific capacity and the first cycle efficiency. The electronic conductivity of the as-prepared composite electrode pellet is 3.3×10^{-3} S cm^{-1} (at 2 DC voltage), which may increase dramatically during the cells cycling, due to partial delithiation of $Li_{1-x}CoO_2$ [17]. The SEM micrographs of the composite electrode after 20 cycles (see Fig. S3 in the Supporting information) show an obvious microstructure change in the surface layer of the failed samples (>200 μm). Along with the increase in the thickness of the composite electrodes, more defects and isolated voids appear in the thicker electrodes, which may further decrease the specific capacity and the first cycle efficiency. Nevertheless, on the other hand, the thicker electrodes contain larger amount of active materials, which may give rise to higher surface capacity. For the 200-μm-thick 3-D composite electrode, the surface capacity can reach 9 mAh cm^{-2}, which is much higher than the surface capacity of the electrode used in the previously reported all-solid-state lithium batteries [3–9,13–15].

The cyclic performance of the 3-D composite electrode is shown in Fig. 4c. For the measured 20 cycles, the 100-μm-thick and 200-μm-thick 3-D composite electrodes deliver excellent capacity retention, while capacity fade appears upon further increasing the thickness of the composite electrodes. Given the paradox in the effect of electrode thickness on the capacity and cycle lifetimes,

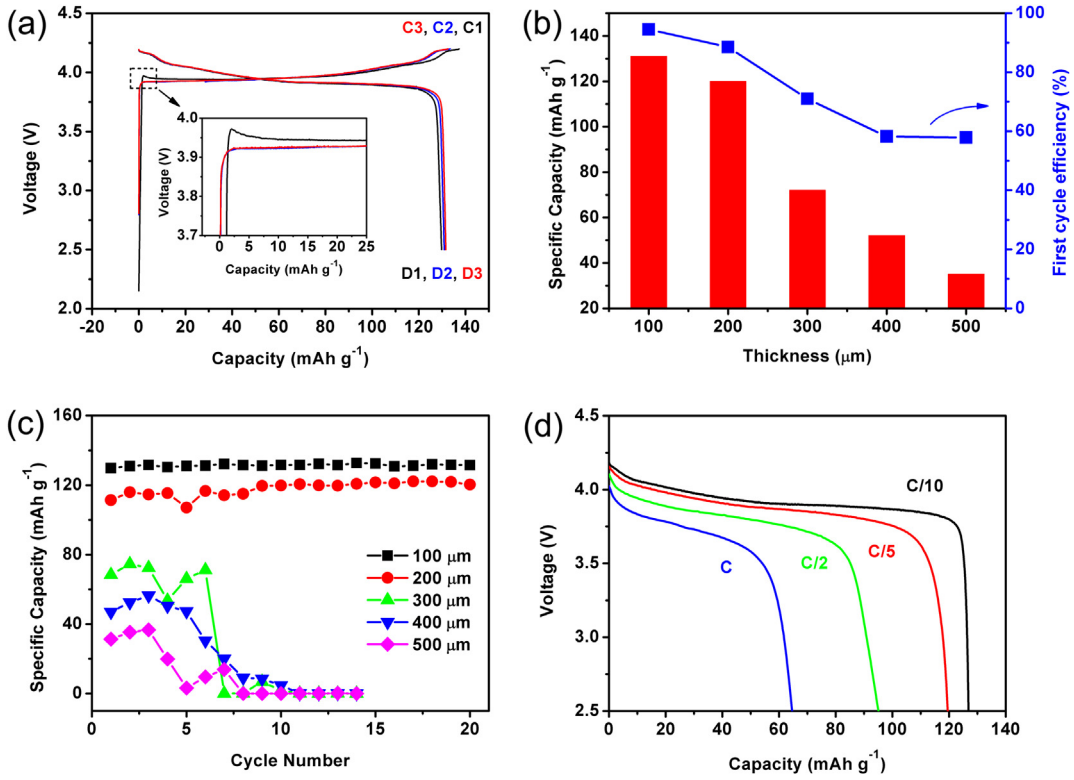

Fig. 4. (a) First three charge/discharge curves obtained from a 100-μm-thick 3-D composite electrode at C/20 charge and discharge rates. The inset shows a small initial polarization spike in the first charging process. (b) Specific capacity and first cycle efficiency of the 3-D composite electrodes with different thicknesses. (c) Cycling of the 3-D composite electrode, tested against a lithium anode over 2.5–4.2 V at C/20. (d) Discharge curves of the cells with100-μm-thick composite electrode at various current rates.

trade-offs need to be made in terms of the electrode thickness. For high-performance cycling properties, the thickness of the 3-D composite electrode should be controlled within 200 μm.

The rate discharge performance of the 100-μm-thick composite electrode is further investigated. As seen in Fig. 4d, though the discharge capacity of the composite electrode decreased with increasing C rates, it still retained relatively high at C/10 (127 mAh g^{-1}), C/5 (120 mAh g^{-1}) and C/2 (95 mAh g^{-1}) rate, which are typical rates in a number of practical applications in portable electronic devices. Even at C rate, the battery delivered a capacity of 65 mAh g^{-1}, which is 47% of the theoretical capacity of $LiCoO_2$.

The high specific capacities and good cycling performances of the composite electrodes may come from the novel 3-D structure and excellent interfaces between the cathode particles and solid state electrolyte. During the sintering and filling process, the melting solid state electrolyte guaranteed excellent interfaces between cathode particles and solid state electrolyte, which were maintained in the final 3-D composite electrodes. In the 3-D structure, the highly conductive $LiCoO_2$ frame provides transport path for electrons in the composite electrode, while the amorphous solid state electrolyte in the interspaces contributes to the ionic conductivity of the composite electrode and strengthens the electrode against the intercalation strains during the electrochemical cycling. Thus new structure design of the composite electrode may provide another way to increase the electronic conductivities. Moreover, the amorphous nature of the $0.44LiBO_2 \cdot 0.56LiF$ solid electrolyte is also favorable for the alleviation of stress originated by the mismatch between the thermal expansion coefficients of cathode and solid electrolyte during the sintering process, leading to improved structural integrity and less imperfections at the cathode/electrolyte interface. The solid electrolyte used here is composed of LiF and $LiBO_2$. It is obvious that the component LiF is stable with lithium foil as F^- cannot be reduced. The component $LiBO_2$ is also stable with lithium as reported by Hensley et al. [18]. Thus, the $0.44LiBO_2 \cdot 0.56LiF$ can also serve as the solid electrolyte layer, which is stable with the lithium foil and most of the negative electrodes used for the all-solid-state lithium batteries.

4. Conclusions

Thus by simple one-step sintering of the laminated $LiCoO_2$ pellet and $0.44LiBO_2 \cdot 0.56LiF$ pellet, high-performance 3-D composite electrodes have been obtained, which possesses a compact structure and contains no electronic conductive additive or polymer binder. During the sintering process, $LiBO_2$ and LiF melt and filled into interspaces of the $LiCoO_2$ frame, forming the compact electrode with a relative density of 92%. The specific capacity of the 3-D composite electrode is dependent on the thickness of the composite electrodes. For the 100-μm-thick 3-D composite electrode, specific discharge capacity of 131 mAh g^{-1} (and surface capacity of 5 mAh cm^{-2}) is obtained at C/20 charge/discharge rate, indicating 96% utilization of the active material, while the 200-μm-thick 3-D composite electrode delivers 88% of the theoretical capacity, i.e., 120 mAh g^{-1}, and its surface capacity can reach 9 mAh cm^{-2}, which is much higher than the surface capacity of the electrode used in the previous all-solid-state lithium batteries. After 20 cycles, the 3-D composite electrodes deliver excellent capacity retention. And even at C/10, C/5 and C/2 rate, the 100-μm-thick composite electrode retains relatively high discharge capacity, which are practical for many portable power applications. Given the low sintering temperature and the amorphous nature of $0.44LiBO_2 \cdot 0.56LiF$ solid electrolyte, this one-step sintering approach is promising to be extended to other cathode systems.

Acknowledgments

This work was supported by the NSF of China (Grant No. 51221291, 51102142 and 51222204) and the Foundation for the Authors of National Excellent Doctoral Dissertations of China (Grant No. 201144).

Appendix A. Supplementary data

Supplementary data related to this article can be found at http://dx.doi.org/10.1016/j.jpowsour.2013.10.113.

References

[1] N.-S. Choi, Z. Chen, S.A. Freunberger, X. Ji, Y.-K. Sun, K. Amine, G. Yushin, L.F. Nazar, J. Cho, P.G. Bruce, Angew. Chem. Int. Ed. 51 (2012) 2–33.
[2] J.B. Goodenough, Y. Kim, Chem. Mater. 22 (2010) 587–603.
[3] N. Kuwata, N. Iwagami, Y. Tanji, Y. Matsuda, J. Kawamura, J. Electrochem. Soc. 157 (2010) A521–A527.
[4] H. Yim, W.Y. Kong, Y.C. Kim, S.-J. Yoon, J.-W. Choi, J. Solid State Chem. 196 (2012) 288–292.
[5] J.F.M. Oudenhoven, L. Baggetto, P.H.L. Notten, Adv. Energy Mater. 1 (2011) 10–33.
[6] L. Baggetto, R.A.H. Niessen, F. Roozeboom, P.H.L. Notten, Adv. Funct. Mater. 18 (2008) 1057–1066.
[7] M. Takahashi, M. Hayashi, T. Shodai, J. Power Sources 189 (2009) 191–196.
[8] Y.-N. Zhou, M.-Z. Xue, Z.-W. Fu, J. Power Sourc. 234 (2013) 310–332.
[9] N.J. Dudney, Mater. Sci. Eng. B 116 (2005) 245–249.
[10] A. Vu, Y. Qian, A. Stein, Adv. Energy Mater. 2 (2012) 1056–1085.
[11] L. Zhang, H. Xiang, Z. Li, H. Wang, J. Power Sources 203 (2012) 121–125.
[12] W. Lai, C.K. Erdonmez, T.F. Marinis, C.K. Bjune, N.J. Dudney, F. Xu, R. Wartena, Y.-M. Chiang, Adv. Mater. 22 (2010) E139–E144.
[13] S. Ohta, S. Komagata, J. Seki, T. Saeki, S. Morishita, T. Asaoka, J. Power Sources 238 (2013) 53–56.
[14] G. Delaizir, V. Viallet, A. Aboulaich, R. Bouchet, L. Tortet, V. Seznec, M. Morcrette, J.-M. Tarascon, P. Rozier, M. Dollé, Adv. Funct. Mater. 22 (2012) 2140–2147.
[15] Z. Zheng, Y. Wang, J. Electrochem. Soc. 159 (2012) A1278–A1282.
[16] P. Birke, F. Salam, S. Döring, W. Weppner, Solid State Ionics 188 (1999) 149–157.
[17] J. Molenda, A. Stoklosa, T. Bak, Solid State Ionics 36 (1989) 53–58.
[18] D.A. Hensley, S.H. Garofalini, Appl. Surf. Sci. 81 (1994) 331–339.